

Effect of Density Control and Impurity Transport on Internal Transport Barrier Formation in Tokamak Plasma^{*)}

Tomoyuki YAMAKAMI, Takaaki FUJITA, Hideki ARIMOTO and Kozo YAMAZAKI¹⁾

Nagoya University, Furo-cho, Chikusa-ku, Nagoya 464-8603, Japan

¹⁾*Nagoya University Professor Emeritus*

(Received 10 December 2013 / Accepted 25 February 2014)

In future fusion reactors, density control, such as fueling by pellet injection, is an effective method to control the formation of the internal transport barrier (ITB) in reversed magnetic shear plasma, which can improve plasma performance. On the other hand, an operation with ITB can cause accumulation of impurities inside the core ITB region. We studied the relation between pellet injection and ITB formation and the effect of impurity transport on the core of ITB for tokamak plasmas by using the toroidal transport analysis linkage. For ITB formation, we showed that the pellet has to be injected beyond the position where the safety factor q takes the minimum value. We confirmed that the accumulation of impurities causes the attenuation of ITB owing to radiation loss inside the ITB region. Moreover, in terms of the divertor heat flux reduction by impurity gas, the line radiation loss is high for high-Z noble gas impurities, such as Kr, whereas factor Q decreases slightly.

© 2014 The Japan Society of Plasma Science and Nuclear Fusion Research

Keywords: internal transport barrier, impurity transport, pellet injection, tokamak reactor, high-Z impurity

DOI: 10.1585/pfr.9.3403091

1. Introduction

The internal transport barrier (ITB) forms in tokamak plasmas with reversed magnetic shear. Plasma confinement is expected to highly improve in the core plasma with ITB. To obtain high confinement while maintaining macroscopic stability, appropriate control of the ITB region and the local pressure gradient is necessary. The self-burning mechanism is presumably the main process of plasma heating in future reactors; however, controlling plasma temperature and current density profiles by only external heating and current drive methods is difficult. Therefore, density control, such as pellet injection, is considered an effective method to control the ITB formation in future self-burning plasmas. Another concern in ITB plasmas is the possibility that impurity ions will accumulate inside the core ITB region, which can then seriously affect the plasma performance, i.e., Ar and Ne injected into the plasma edge reduce W and C from the plasma-facing components, and the divertor heat loads by radiative cooling. Therefore, it is important to study the effect of density control and impurity transport on the ITB plasma.

ITB formation by pellet injection and the feasibility of pellet injection has already been analyzed in tokamak fusion reactor [1]. In this study, we discuss the conditions of ITB formation in detail. Furthermore, the effect of impurities on ITB structure and plasma performance is analyzed. We used the 1.5-dimensional (1.5-D) transport code, i.e., toroidal transport analysis linkage (TOTAL) [2, 3], to sim-

ulate the radial distribution and time evolution of plasma parameters and impurity ions. In section 2, we present the transport and impurity transport models. The simulation results are discussed in section 3 and the conclusions are summarized in section 4.

2. Simulation Models

2.1 Transport model and pellet injection model

The formation of the ITB is explained as the suppression of the ion temperature gradient (ITG) turbulence owing to the $E \times B$ shear flow. In this study, as transport model, we used the mixed Bohm/gyro-Bohm [4, 5] transport model with $E \times B$ shear stabilization of ITG, which reproduces the ITB formation in H-mode plasma. The $E \times B$ flow shearing rate $\omega_{E \times B}$ is defined as [6, 7]

$$\omega_{E \times B} \cong \left| \frac{RB_\theta}{B_\phi} \frac{\partial}{\partial r} \left(\frac{E_r}{RB_\theta} \right) \right|, \quad (1)$$

where E_r , B_θ , and B_ϕ are the radial electric field, the poloidal, and toroidal magnetic field, respectively. In tokamak plasmas, the radial electric field E_r is not easily determined. Therefore, in this study, E_r is described simply as

$$\frac{dE_r}{dr} \cong -\frac{1}{en_i^2} \frac{dn_i}{dr} \frac{dp_i}{dr}, \quad (2)$$

under the H-mode condition [8], where n_i and p_i are the ion density and ion pressure, respectively. The ITG growth rate γ_{ITG} is defined as [9]

author's e-mail: tomoyuki0610@gmail.com

^{*)} This article is based on the presentation at the 23rd International Toki Conference (ITC23).

$$\gamma_{\text{ITG}} = \frac{(\eta_i - 2/3)^{1/2} |s| c_i}{qR}, \quad (3)$$

where $\eta_i = L_n/L_T$, $L_n^{-1} = -\nabla n/n$, $L_T^{-1} = -\nabla T_i/T_i$, $c_i = (T_i/m_i)^{1/2}$, and q is the safety factor. s is the magnetic shear, which is defined as

$$s = \frac{r}{q} \left(\frac{dq}{dr} \right). \quad (4)$$

As for pellet injection, we assumed injection from the high magnetic field side (HFS), which is an effective method for central fueling [10]. This model consists of two processes: pellet ablation and mass relocation. For pellet ablation, we used the widely used neutral gas shielding model (NGS). We also modeled the mass relocation caused by the $E \times B$ drift effects. Details of the transport model and pellet injection model used in the simulation are described in ref [1].

2.2 Impurity transport model

For impurity transport in ITB plasma, the rate and diffusion equations, which can calculate the cooling rate, considering ionization and recombination are solved using the IMPDYN [11] code coupled with the ADPAK atomic physics package [12];, which can calculate the cooling rate,

$$\frac{\partial n_k}{\partial t} = -\frac{1}{V'} \frac{\partial}{\partial \rho} (V' \Gamma_k) + [\gamma_{k-1} n_{k-1} + \alpha_{k+1} n_{k+1} - (\gamma_k + \alpha_k) n_k] n_e + S, \quad (5)$$

and

$$\Gamma_k = \Gamma_k^{NC} - D_k^{AN}(\rho) \frac{\partial n_k}{\partial \rho} + V_k(\rho) n_k, \quad (6)$$

where γ_k is the ionization rate, α_k is the recombination rate, and S_k is the particle source term. Γ_k^{NC} and D_k^{AN} are the neoclassical part of the impurity flux and anomalous part of the diffusion coefficient, respectively. In the simulation, we used a constant D_k and simply modeled the impurity velocity $V_k = V_k(a)(r/a)$ to reproduce the anomalous impurity transport, in which $V_k < 0$ corresponds to the inward velocity. The main fuel neutrals are calculated by the AU-RORA Monte Carlo code [13].

The neoclassical impurity flux in tokamak plasma is described as

$$\Gamma_k^{NC} = -D_k^{NC} \nabla n_k + D_k^{NC} n_k \left[\sum_{l \neq k} (g_{nl \rightarrow k} \nabla n_l / n_l) + g_{T_i} \nabla T_i / T_i + g_{T_e} \nabla T_e / T_e \right], \quad (7)$$

where n_k and D_k^{NC} are the density and particle diffusion coefficients, respectively, of the k -th ionic charge state of the impurity. g_{n_i} , g_{T_i} , and g_{T_e} denote the screening or pinch effects of the density gradient, the ion temperature gradient, and the electron temperature gradient, respectively.

The impurity source is defined as the impurity neutral flux on the plasma boundary. The neutral impurity density profile $n_0(\rho)$ is assumed to be

$$n_0(\rho) = -\frac{V'(1)\Gamma_0(1)}{V'(\rho)v_0} \exp\left(-\frac{1}{V'} \int_1^\rho d\rho n_e(\rho)\right), \quad (8)$$

derived from

$$\frac{\partial n_0}{\partial t} = -\frac{1}{V'} \frac{\partial}{\partial \rho} (V' \Gamma_0) - \gamma_0 n_e n_0 \approx 0, \quad (9)$$

$$\Gamma_0(\rho) \approx -n_0(\rho) v_0, \quad (10)$$

$\Gamma_0(1)$ is the neutral impurity flux at the plasma boundary ($\rho = 1$) and v_0 is the neutral impurity inward velocity (assuming an energy of 10 eV). The symbols γ_0 and n_e denote the ionization coefficient and electron density near the plasma boundary, respectively.

3. Simulation Results

In this study, we assumed the operation conditions in the self-burning tokamak fusion reactor. The reactor parameters ($R_p = 5.29$ m, $a_p = 1.25$ m, $B_t = 7.11$ T, and $I_p = 13$ MA) are obtained from the reactor design system code PEC (Physics Engineering Cost) [2]. In the simulation, the safety factor profile with reversed shear was assumed and it was fixed in time, and the time evolution of density and temperature was analyzed by using the transport model. The external heating power was given in a fixed profile, together with the α -heating power, from deuterium–tritium fusion.

3.1 Effect of pellet injection on ITB formation

The simulation of the ITB formation by pellet injection was previously reported [1]. The process was analyzed in detail to elucidate the ITB formation mechanism. Figure 1 (a) shows the time evolution of the α -particle heating

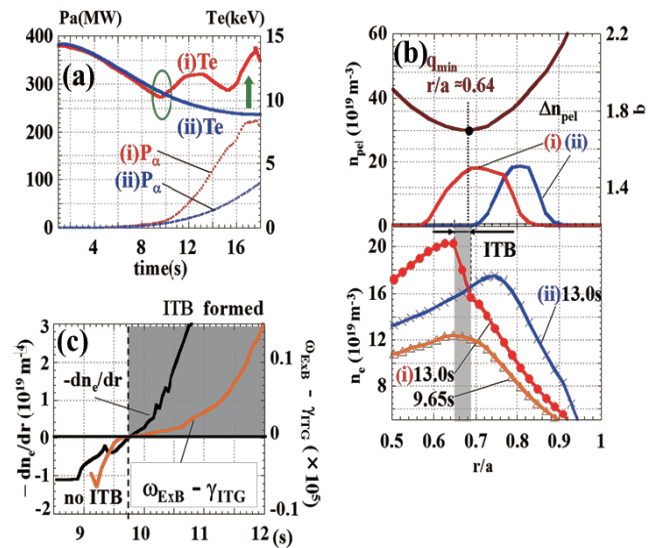


Fig. 1 (a) Time evolution of the α -particle heating power P_α and electron temperature T_e . (b) Radial profile of the pellet deposition Δn_{pel} , electron density n_e , and safety factor q . (c) Time evolution of the n_e gradient $-dn_e/dr$ and stability condition $\omega_{E \times B} - \gamma_{\text{ITG}}$ at q_{min} for condition (i).

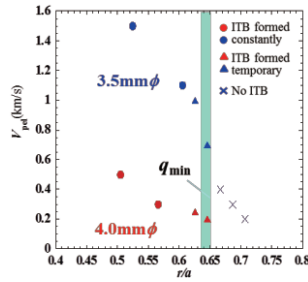


Fig. 2 Relation of the pellet arrival position and ITB formation.

power P_α and volume average electron temperature T_e at two pellet injection conditions: (i) 4 mm $\phi - 0.3$ km/s and (ii) 3.5 mm $\phi - 0.3$ km/s. The pellets were injected from the HFS. In condition (i), T_e started to rise at $t = 10$ s, while such behavior was not observed for condition (ii). The radial profile of pellet deposition and electron density n_e in conditions (i) and (ii) are shown in Fig. 1 (b). The radial profile of safety factor q is also described. Factor q takes its minimum value q_{\min} (i.e., magnetic shear $s = 0$) at $ca. r/a = 0.64$. Pellets are injected deeper in condition (i). This is because pellet ablation time is shorter for smaller size pellets in super-high temperature plasma. Figure 1 (c) shows the time evolution of the electron density gradient $-dn_e/dr$ and the ITG stabilization condition $\omega_{E \times B} - \gamma_{ITG}$ at the q_{\min} position in condition (i). When the pellet is injected beyond the q_{\min} position, the density gradient turns to positive values at q_{\min} , as in Fig. 1 (c), which means that the gradient towards the center of the plasma increases as in Fig. 1 (b). Then, the $E \times B$ shear flow exceeds the ITG growth rate ($\omega_{E \times B} > \gamma_{ITG}$) and the ITG mode is stabilized. This mechanism leads to the ITB formation. In contrast, for pellet injection to the outer side of the q_{\min} position as in condition (ii), ITB formation is not observed even with the lapse of time. Figure 2 shows the relation of pellet injection condition and pellet arrival position. The maximal position where the pellet reached inside is defined as the pellet arrival position. The ITB formed constantly with the injection condition is marked by the circle, while for that formed temporarily the position is marked by the triangle. This occurred because the q profile changed with time and the q_{\min} position moved slightly inward. Therefore, the pellet did not reach the q_{\min} position and ITB could not be maintained. From the results, we concluded that “pellet injection beyond the q_{\min} position” is required for ITB formation.

3.2 Effect of impurity transport on tokamak ITB plasma

First, we analyzed the effect of high-Z impurity ions on the plasma parameters and ITB structure. Before injecting the impurity into the plasma, steady-state burning plasma conditions were established without impurities as shown in Fig. 3 (a) ($t < 70$ s). P_α is fixed to 500 MW by

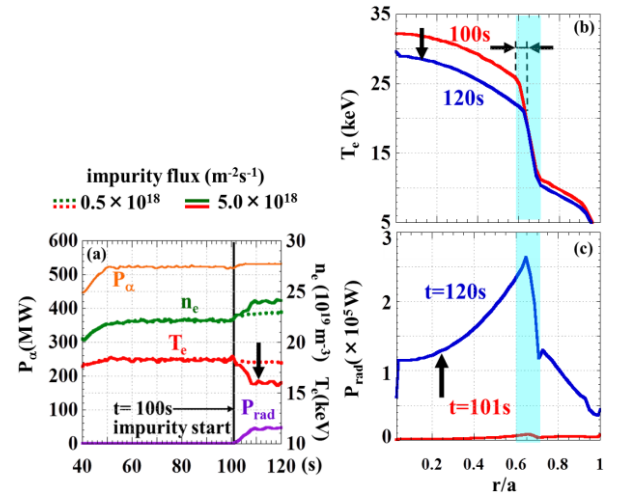


Fig. 3 (a) Time evolution of P_α , n_e , T_e , and line radiation loss P_{rad} . (b) and (c) Radial profile of T_e and P_{rad} for the case of higher impurity flux (5.0×10^{18}).

the electron density feedback control and the external heating power feedback control. Then, a continuous neutral tungsten impurity influx was introduced at $t = 100$ s.

Figure 3 (a) shows the time evolution of P_α , n_e , T_e , and line radiation loss P_{rad} . Figure 3 (b) shows the change in the radial profile of the electron temperature. The dotted and solid lines correspond to different quantities of impurity influx ($\text{m}^{-2}\text{s}^{-1}$): 0.5×10^{18} for the dotted line and 5.0×10^{18} for the solid line. In the case of the lower impurity concentration shown by the dotted lines, no significant fluctuation is observed in the plasma parameters. However, in the case of higher impurity concentration, the ITB region narrowed and the core plasma temperature decreased. The increased radiation loss owing to the increased tungsten impurity concentration in the ITB region (Fig. 3 (c)) probably caused the decrease in heat flux and then the $E \times B$ shear flow. Presumably, radiation loss affects the ITB formation even if it is smaller than the α -heating power.

In this section, we also investigated the effect of radiation loss caused by noble gas impurity ions on the fusion reactor performance. Steady-state burning plasma condition with $P_\alpha = 500$ MW is established by fixing the electron density as shown in Fig. 4 (a). The α -heating power P_α is feedback-controlled by the external heating power P_{rf} . Noble gas (Ne, Ar, and Kr) impurity influx is introduced at $t = 70 - 100$ s. Figure 4 (b) shows the ignition margin M versus P_{rad} at the time the plasma returned to steady state after introducing the impurity influx (dotted line in Fig. 4 (a)). Factor M is defined as $M = P_\alpha / (P_\alpha + P_{\text{rf}})$ and therefore $M = 1$ is equivalent to the ignition or fusion energy gain factor $Q = \infty$. The impurity flux quantity was scanned until M drops to approximately 0.8 for Ne, Ar, and Kr. For divertor heat flux mitigation by impurity radiative cooling, it is desirable to obtain large line radiation loss at the plasma edge while sustaining high Q values. When low-Z impurity ions are introduced, such as Ne and Ar,

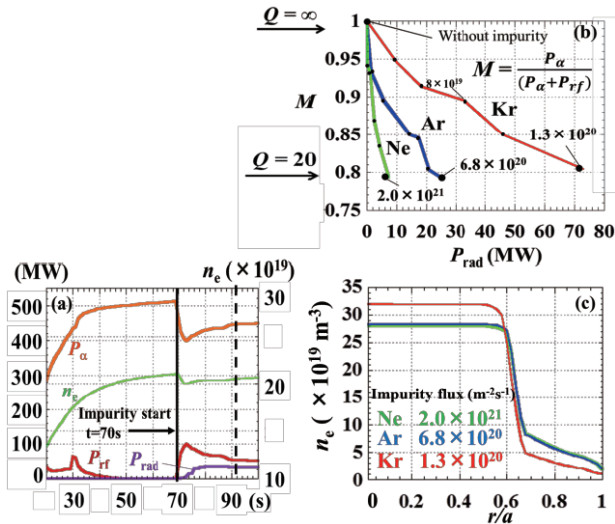


Fig. 4 (a) Time evolution of P_α , n_e , P_{rf} and P_{rad} . (b) Ignition margin M versus P_{rad} at steady-state after impurity is introduced (dotted line in Fig. 4 (a)) (c) Radial profile of n_e after impurity is introduced.

only small radiation loss is produced for $0.8 < M < 1$. Because these ions have relatively small radiation power per ion in the reactor plasma temperature, and hence a large amount of ions should be introduced in the plasma before obtaining high line radiation loss. Even with small radiation, factor M falls to approximately 0.8. A possible reason for the degradation of M even with small radiation loss is the change in the n_e profile owing to the high impurity influx. As shown in Fig. 4 (c), the electron density outside the ITB region increased in the case of Ne and Ar after impurities were introduced. Therefore, because the average n_e is fixed, n_e inside the ITB region decreased and this minimizes Q . In contrast, when Kr is introduced, larger radiation loss is obtained with lower impurity concentration compared to the low-Z impurities for the same level of Q . In this case, no effect to the density profile is observed and

the degradation of M seems to be caused mainly by the increase in the radiation loss.

4. Summary

We simulated the effect of pellet injection and impurity transport to ITB plasma in tokamak reactor. By altering the pellet injection condition, we clarified that pellet must be injected beyond the q_{min} position to form ITB in the tokamak reversed shear plasma. For the effect of impurity transport to ITB plasma, it is shown that the radiation loss affects the ITB structure and plasma parameter, even if it is relatively smaller than P_α . In addition, for the impurity transport, it is confirmed that high-Z noble gas impurities can produce line radiation loss with lower impurity concentration compared to low-Z impurities for the same level of Q .

Acknowledgments

This work was partially supported by JSPS Grants-in-Aid for Scientific Research Grant Number 25420895.

- [1] T. Yamakami *et al.*, Plasma Fusion Res. **8**, 2403079 (2013).
- [2] K. Yamazaki and T. Amano, Nucl. Fusion **32**, 633 (1992).
- [3] K. Yamazaki *et al.*, Fusion Eng. Des. **81**, 2743 (2006).
- [4] T. Tara *et al.*, Plasma Phys. Control. Fusion **43**, 507 (2001).
- [5] J. Garcia, K. Yamazaki, J. Dies and J. Izquierdo, Phys. Rev. Lett. **96**, 105007 (2006).
- [6] T.S. Hahm and K.H. Burrell, Phys. Plasmas **2**, 1648 (1995).
- [7] P. Zhou, W. Horton and H. Sugama, Phys. Plasmas **6**, 2503 (1990).
- [8] F.L. Hinton and G.M. Staebler, Phys. Fluids B **5**, 1281 (1993).
- [9] B. Esposito *et al.*, Plasma Phys. Control. Fusion **45**, 933 (2003).
- [10] P.T. Lang *et al.*, Phys. Rev. Lett. **79**, 1478 (1997).
- [11] T. Amano, J. Mizuno and J. Kako, Internal report IPPJ-616, Institute of Plasma Physics, Nagoya Univ. (1982).
- [12] R.A. Hulse, Nucl. Technol. Fusion **3**, 259 (1983).
- [13] M.H. Huges and D.E. Post, J. Comput. Phys. **28**, 43 (1978).